ACS APPLIED MATERIALS & INTERFACES

Article

Rational Design of Hierarchical Carbon/Mesoporous Silicon Composite Sponges as High-Performance Flexible Energy Storage Electrodes

Yanbing Yang, Xiangdong Yang, Shasha Chen, Mingchu Zou, Zhihao Li, Anyuan Cao, and Quan Yuan

ACS Appl. Mater. Interfaces, **Just Accepted Manuscript** • DOI: 10.1021/acsami.7b05032 • Publication Date (Web): 22 Jun 2017

Just Accepted

ACS Publications

ACS Applied Materials & Interfaces is published by the American Chemical Society.
1155 Sixteenth Street N.W., Washington, DC 20036

Rational Design of Hierarchical Carbon/Mesoporous Silicon Composite Sponges as High-Performance Flexible Energy Storage Electrodes

Yanbing Yang,[1] Xiangdong Yang,[1] Shasha Chen,[1] Mingchu Zou,[2] Zhihao Li,[1] Anyuan Cao[2] and Quan Yuan*[1]*

[1]Key Laboratory of Analytical Chemistry for Biology and Medicine (Ministry of Education), College of Chemistry and Molecular Sciences, Wuhan University, Wuhan 430072, China

[2]Department of Materials Science and Engineering, College of Engineering, Peking University, Beijing 100871, China

KEYWORDS: Hierarchical, CNT, mesoporous Si, flexible, lithium-ion battery

Corresponding Author: *E-mail: anyuan@pku.edu.cn; yuanquan@whu.edu.cn

ABSTRACT

Nanostructuring silicon (Si) and combining Si with carbon shells have been studied in recent Li-ion battery electrodes, yet it remains a grand challenge to overcome the low electrical conductivity and associated volume change of Si. Here, by first coating a mesoporous SiO_2 (meso-SiO_2) onto carbon nanotube (CNT) networks and then converting it into a meso-Si layer covered by carbon, we obtained a freestanding, highly porous composite sponge electrode consisting of three-dimensionally interconnected sandwiched carbon-Si-CNT skeletons. In this hierarchical structure, the macropores among the sponge connect to mesopores in the meso-Si layer so that Li^+ diffusion is facilitated, while the underlying CNT networks serve as conductive paths for electrons transport. Meanwhile, the outer carbon coating on meso-Si could buffer the volume expansion and prevent material shedding. As a result, our sandwiched carbon-Si-CNT electrodes exhibit large specific capacity, high rate capability and long cycle life. Combination of carbon-wrapped meso-Si and CNT sponges might be a potential strategy for developing efficient electrodes in various energy storage systems.

INTRODUCTION

Lithium ions batteries LIBs (LIBs) have become an important class of energy storage devices and found wide applications in electronic devices and electric vehicles.[1, 2] As a key component, electrode materials in the LIBs provide active sites for energy storage and dominate the electrochemical activity. Owing to its large theoretical capacity (4200 mAh g^{-1}), low Li-uptake voltage, abundant resource and high safety, silicon-based electrodes have attracted remarkable attention for their potential application as anodes in high energy density and power performance LIBs.[3–6] However, two problems exist in silicon (Si) electrode upon the Li insertion and extraction during the charge/discharge processes: the large volume change during the Li insertion process, which often leads to the structure fracture and pulverization and finally the damage of the mechanical integrity of the electrode, and the inherent poor electrical conductivity of Si electrode. Engineering of Si nanostructures with void space[7–11] or coating a conductive buffer layer[12–22] has been recognized as an efficient approach to buffer the volume expansion, prevent fracture, and improve conductivity. Recently, Zhao *et al.* fabricated a mesoporous C/Si composites with ultrasmall Si nanoparticles embedded in the mesoporous C framework to alleviate the volume expansion of Si during Li insertion.[23] As a further step, Ruoff *et al.* demonstrated a Si-based anode by anchoring graphene encapsulated Si nanoparticles on graphite foam to increase the Si mass loading and the specific capacity.[13]

Though significant improvements in the electrochemical properties have been reported, the above mentioned Si-based composite electrodes suffered either from low porosity or poor electrode geometry in which a traditional LIB electrode is prepared by mixing the active

materials with binder and conductive additives. The diffusion rate of Li^+ between the electrolyte and Si can be significantly hindered due to the limited porosity structure, which leads to reduced capacity and rate capability. The addition of inactive, insulate and swelling polymer binders in the electrode fabrication process disturbs the interconnected network and decreases the electrode conductivity as well as increases the total mass of the whole electrode, and makes it difficult to realize high power density and energy density LIBs. Furthermore, the composite electrode undergoes structure fracture and pulverization due to the poor mechanical performance. In this regard, it is still challenging to prepare porous Si-based nanostrcutures with both well-controlled porosity and highly conductive electrons channels as well as superior flexibility.

Here, we demonstrate a flexible three-dimensional (3D) porous LIBs electrode by coating a uniform carbon-wrapped mesoporous Si (meso-Si) throughout a CNT sponge. The obtained hierarchical porous structure based on a CNT network can facilitate Li^+ diffusion, fast electron and ion transportation. More importantly, the presence of a carbon coating on meso-Si accommodates volume expansion, maintains the electrode integrity and enhances the electrical conductivity of the Si electrode. When used as LIBs electrode, the CNT/meso-Si/C 3D porous network shows large specific capacity, high rate capability and long cycle stability. The integration of meso-Si and CNT sponge to fabricate flexible 3D hierarchical porous architecture not only represents a method for constructing porous functional materials but also provides a pathway for realizing high performance energy storage systems.

EXPERIMENTAL SECTION

Synthesis of CNT sponges. The CNT sponges were synthesized by chemical vapor deposition approach, as described in our earlier report.[24] Specifically, ferrocene and 1,2-dichlorobenzene were used as the catalyst and carbon source, respectively. The mixture solution was injected into the furnace by a syringe pump at a feeding rate of 0.13 mL min^{-1}. The carrier gases were composed of Ar (2000 mL min^{-1}) and H_2 (300 mL min^{-1}). CNT sponges were deposited on the quartz substrate and formed a sponge structure. The CNT sponges can be directly use after scraping from the substrate.

Synthesis of CNT/meso-SiO_2 composite sponges. The core-shell structured CNT/meso-SiO_2 nanocomposite was synthesized by a sol-gel method according to our previous report.[25] In a typical preparation, the CNT sponges were immersed in the meso-SiO_2 precursor solution which was composed of CTAB template, ethanol, water, ammonia and TEOS for 3 to 5 times at 1 hour interval under continuous shaking. The different immersion times result in the CNT/meso-SiO_2 nanocomposite with different meso-SiO_2 shell thicknesses. The obtained CNT/meso-SiO_2 sponges were then immersed in the deionized water to remove the residual precursors. It is worth mentioning that the CTAB cannot remove from the core-shell structure in the washing process. After subsequent freeze drying, a core-shell structure with CNT as core and meso-SiO_2 as shell was obtained.

Fabrication of CNT/meso-Si/C sponges. The CNT/meso-Si/C sponge was synthesized by a magnesiothermic reduction method. Specifically, the core-shell structured CNT/meso-SiO_2 nanocomposites and 0.2 g of metal Mg powder were put into the porcelain boat. The boat was then placed in the tubular furnace. The furnace was heated to 700 ^{o}C for 2 hours under Ar atmosphere containing 10% H_2. The ramping rate was kept at 5 ^{o}C min^{-1}. After cooling to room temperature, the

CNT/meso-Si/C sandwiched nanocomposite was obtained after washed with 1 M HCl for one night to remove the Mg residues and freeze dried for 12 hours.

Characterization. TEM images were obtained on a FEI Tecnai G2 F20 (Tecnai F20) operated at 200 kV. High-angle annular dark-field scanning transmission electron microscopy and elemental mapping were recorded on a TEM (JEOL ARM200f). The CNT and CNT/meso-Si/C sample were dispersed in ethanol by ultrasonic and finally collected by copper grids for TEM observation. SEM characterization was performed on a Hitachi S-4800 microscope (Hitachi, Japan). Raman spectra were recorded using a RM 2000 Microscopic Confocal Raman Spectrometer (Renishaw PLC, England) with a 514 nm laser. The samples were prepared on Si wafers for Raman measurements. TGA analysis was taken on a TGA Q5000 analyzer from 20 to 800 ^{o}C under air with a heating rate of 20 ^{o}C min^{-1}. Nitrogen sorption isotherms were measured at 77 K using ASAP 2010 analyzer (Micromeritics). Before measurements, all of the samples were degassed in vacuum at 150 ^{o}C for 12 h. Mechanical measurements on CNT and CNT/meso-Si/C spones were carried out by a single-column static instrument (Instron 5843) equipped with two flat compression stages and a 10 N load cell. The crystal structure of the CNT and CNT/meso-Si/C were obtained on an X-ray diffractometer (Bruker, D8 Advance, Germany).

Electrochemical measurements. The CNT and synthesized CNT/meso-Si/C sponge were directly used as the electrode of Li-ions battery without any conductive additive and binding agent. Specifically, the CNT or CNT/meso-Si/C sponges were first dried at 60 ^{o}C for 24 hours to remove the adsorbed water. The mass of the electrode material (CNT sponge and CNT/meso-Si/C sponge) used in the Li-ions battery is typically 5~10 mg. The cell measurements were performed using coin-type cells. Li ions batteries were assembled in the Ar filled glovebox with oxygen and water

contents less than 1 ppm. The cells were assembled with a stainless steel anode shell, a metallic lithium foil anode (0.5 mm thick), a polypropylene separator (Celgard 2400), a piece of CNT or CNT/meso-Si/C positive electrode, and a stainless steel cathode shell. The electrolyte was composed of 1 M $LiPF_6$, ethyl methylcarbonate (EMC), ethylene carbonate (EC) and dimethylcarbonate (DMC). The galvanostatic discharge-charge performance of the cells was measured by a Land CT2001A battery system at various current densities within a voltage range from 0.05 to 1.5 V. The cycling performance was studied under a current density of 500 mA g^{-1}. The gravimetric current density and specific capacity were calculated by the whole electrode material including CNT and meso-Si.

RESULTS AND DISCUSSIONS

Our design principle and synthetic route toward CNT/meso-Si/C 3D porous network is illustrated in Figure 1a. Firstly, the CNT/meso-SiO_2 core-shell nanocomposites were prepared by a sol-gel method as described in our previous work.[25] Specifically, the CNT sponge was dipped in the meso-SiO_2 precursor solution and served as the substrate for nucleation and formation of meso-SiO_2. Secondly, a magnesiothermic reduction process was performed at 700 ^oC under reduced atmosphere. In this process, the meso-SiO_2 layer was reduced to interconnected meso-Si nanoparticles, while the cetyltrimethyl ammonium bromide (CTAB) in the CNT/meso-SiO_2 sponge was converted to carbon layer coated on the meso-Si. By this way, a sandwiched CNT/meso-Si/C architecture composed of CNT porous network and carbon-wrapped meso-Si was obtained. It is worth mentioning that the bulk CNT/meso-Si/C sponges are mechanically robust. The CNT/meso-Si/C sponges can be compressed to large deformations without collapsing and then recover to original shape (Figure 1b).

The excellent mechanical performance of the CNT/meso-Si/C sponges is attributed to the presence of a flexible and robust CNT network.

Scanning electron microscopy (SEM) and transmission electron microscopy (TEM) images reveal two features related to the morphology and structure of our composite sponges (Figure 2a–2d). First, the meso-SiO_2 and carbon-wrapped meso-Si are uniformly coated on the CNT sponge and the coating thickness can be well controlled. Second, the highly interconnected porous 3D structure are well maintained before (Figure S1) and after coating of carbon-wrapped meso-Si (Figure 2b). The original CNTs have a smooth surface with diameter around 30 nm (Figure S1). After coating carbon-wrapped meso-Si, the CNT surface becomes rough and the diameter increases to about 50 nm (Figure 2b). The interface between CNT and meso-Si/C are clearly observed at regions where CNTs are protruded from the meso-Si/C layer, indicating that the core-shell structure was successfully obtained (Figure 2b). The core-shell structure of CNT/meso-Si/C nanostructure can be further evidenced by TEM image (Figure 2d). From the TEM image, it also can be observed that the CNT/meso-Si has a rough surface consisting of closely stacked Si nanoparticles arranged along the CNT surface, indicating that the crystallization process has occurred (Figure 2d). The thickness of the meso-Si layer on the CNT surface is estimated to be 8–10 nm, consistent with the SEM images. It is worth mentioning that the presence of large carbon aggregates on the meso-Si surface is due to the presence of excess CTAB in the CNT/meso-SiO_2 sponge. Here, the sol-gel method ensures the conformal and smooth coating of meso-SiO_2 layer on the CNT surface in a controlled manner (Figure S2), thus enabling the formation of uniform CNT/meso-Si/C sandwiched structure with different thicknesses (Figure S3). High resolution TEM image clearly reveals the crystalline fringes interconnected by crystallized domains with the interlayer spacing of 0.31 nm (Figure 2e, 2f).

Furthermore, the smooth and flexible carbon layer covered on the surface of meso-Si is clearly observed. X-ray diffraction (XRD) was performed to further confirm the successful formation of meso-Si layer (Figure 2g). It can be seen that the original CNT sponge only displays two diffraction peaks corresponding to (002) and (101) crystal planes. The meso-Si coating layer induced the presence of well-resolved crystal planes of Si phase (JCPDS number 27–1402), indicating that the meso-SiO_2 is successfully converted into meso-Si by the magnesiothermic reduction reaction. Raman spectra in Figure 2h shows that the peak present at around 512 cm^{-1} in the CNT/meso-Si/C composite is attributed to the characteristic scattering of the first-order optical phonon of Si.[26, 27] Additionally, a broad peak is present at about 965.5 cm^{-1}, which can be ascribed to the scattering of transverse optical phonon.[24, 28] The above results demonstrate that the meso-Si is successfully coated on the CNT surface. To confirm the uniform coating of meso-Si on CNT, dark field measurements and corresponding elemental mappings of carbon and Si were conducted (Figure 2i). Results demonstrate that the CNT cavity is clearly observed and the Si coating layer is homogeneously distributed throughout the CNT surface. In addition, the presence of carbon signal throughout the composite nanotube indicates that the surface coating of carbon was successfully obtained. The above results demonstrate that the nanostructure of uniform CNT/meso-Si/C is obtained with the proposed method.

From the thermogravimetric analysis (TGA) curves in Figure S4, it can be observed that the pristine CNT sponge undergoes a fast gravimetric loss at a combustion temperature of 500 ^{o}C in air, with about 15% of residue weight derived from the oxidized iron catalyst (Figure S4). After meso-Si/C coating, the weight loss is delayed to 550 ^{o}C due to the shielding and protecting effect of meso-Si/C layer. The TGA curves also indicate that the weight loading of meso-Si is about 50–55%

in the CNT/meso-Si/C composite sponge. The weight ratio of surface coated carbon layer on the meso-Si surface was quantified to be about 2% as evidenced from the energy-dispersive X-ray spectrometer (EDX) analysis in Figure S5. N_2 adsorption-desorption curves of the CNT and meso-Si/C coated CNT sponges indicate that the Brunauer-Emmett-Teller (BET) surface area has increased from 62 $m^2 g^{-1}$ for CNT sponge to 93 $m^2 g^{-1}$ for CNT/meso-Si/C sponge with a total pore volume of 0.26 $cm^3 g^{-1}$ (Figure S6). The pore size distribution curves in Figure S6 show narrow size distribution at around 3 nm in diameter and the increased percentage of mesopores after meso-Si/C coating. The increased surface area and mesopores ratio are due to the introduction of a meso-Si layer into the macroporous network.

The pure Si nanostructures are typically very fragile and collapse easily under modest compression or deformation.[29, 30] The incorporation of flexible CNT sponge into the macroscopic structure of meso-Si significantly improved the mechanical performance. Similar to the pure CNT sponge, the CNT/meso-Si/C sponge can be compressed to large strains (up to 60%) and recovers to the original shape after releasing the loading as observed from the compressive stress-strain (σ-ε) curves (Figure S7, S8). In addition, the CNT/meso-Si/C sponge shows relatively higher compressive stresses than the CNT sponge at all investigated stresses, indicating that the coating of meso-Si mechanically reinforce the CNT network. From the σ-ε curves in Figure S7, it can be seen that the CNT/meso-Si/C sponge can be compressed to large strains of 40% for 1000 cycles without stress degradation or structural damage. The excellent mechanical performance of CNT/meso-Si/C composite sponge is crucial to its application in energy storage systems.

In the hierarchical structured CNT/meso-Si/C composite sponge, the macropores exist between the nanotubes and mesopores in the meso-Si layer allow easy diffusion of electrolyte and ensure the

meso-Si to be accessible to electrolyte. Meanwhile, the 3D conductive network facilitates electrons transport and serves as mechanical support as well as current collector. Thus, the CNT/meso-Si/C composite sponge with optimized structure can be directly used as freestanding and flexible electrodes of LIBs without binder or conductive additive. The charge and discharge performance of CNT/meso-Si/C sponge as LIBs electrode was investigated at various current densities from 0.1 to 4 A g^{-1}. From the charge and discharge curves (Figure 3a), it can be seen that the CNT/meso-Si/C electrode shows a long plateau below 0.1 V in the first discharge which is ascribed to the Li-alloying process with crystalline Si and the formation of amorphous Li_xSi phase. Additionally, the CNT/meso-Si/C electrode exhibits high capacity performance at all investigated current densities. The initial coulombic efficiency of the CNT/meso-Si/C electrode is 86%. The irreversible capacity is attributed to the formation of solid electrolyte interphase on the surface of electrode and the irreversible insertion of Li^+ ions into the meso-Si.[28] After the first cycle, the charge capacity is close to the discharge capacity at all current densities, demonstrating a 99% coulombic efficiency of the CNT/meso-Si/C electrode. The specific discharge capacity of the nanocomposite at the current density of 0.5 A g^{-1} is 1950 mAh g^{-1}, corresponding to a capacity of 19.5 mAh mL^{-1} with respect to the volume of the electrode. This value is a 510% enhancement of the capacity performance compared to the cell with a pure CNT electrode (320 mAh g^{-1}, Figure S9), indicating that the mesostructure facilitates the high accessibility of the active Si nanoparticles for Li insertion. This improved capacity performance is believed to stem from the highly porosity structure and the direct contact between the CNT and meso-Si, which facilitates the electrolyte and Li^+ transport. Since the Si loading amount is 55%, the theoretical capacity of CNT/meso-Si/C sponge is calculated to be 2450 mAh g^{-1}. Thus, the capacity of CNT/meso-Si/C composite electrode approaches its

theoretical limit. Furthermore, the CNT/meso-Si/C composite electrode exhibits excellent rate performance, in which a discharge capacity of 1700 mAh g^{-1} is still maintained even increasing the current density to 4 A g^{-1} (40 times higher) (Figure 3b). This high rate performance corresponds to a 81% capacity retention with respect to the discharge capacity at 0.1 A g^{-1}, significantly higher than that of CNT/meso-Si electrode (51%) (Figure S10) and pure CNT electrode (31%) (Figure S9). This is the best rate performance that has been reported based on Si electrode, which is typically in the range of 22%–68% (Figure 3c). The high rate performance can be attributed to the following reasons. First, the mesostructured meso-Si/C facilitates electrolyte transport and shortens Li^+ diffusion path. Second, the CNT conductive network and surface carbon coating layer on meso-Si provides an electric pathway for efficient electrons transport and accommodate the huge volume change of meso-Si during the charge/discharge process. The capacity performance of the CNT/meso-Si/C electrode highly depends on the meso-Si mass loading. The CNT/meso-Si/C composites with meso-Si thickness of 5 nm and 10 nm show discharge capacity of 1500 mAh g^{-1} and 1860 mAh g^{-1}, respectively (Figure S11). The reduced discharge capacity of CNT/meso-Si/C with 5 nm thickness is due to the low mass loading of Si and thus the decreased active sites. As for the meso-Si with 10 nm thickness, the presence of cracks during the cycling charge/discharge process that results in the mechanical degradation is the major factor that influences the electrode capacity (Figure S12). The performance enhancement of CNT/meso-Si/C electrode is believed to stem from the synergistic effect between the hierarchical flexible porous network of CNT and the meso-Si active layer.

The cyclic stability of the CNT/meso-Si/C electrode was investigated at a series of current densities (Figure 3d). It can be observed that the discharge capacity remains relatively stable at each

current density during the investigated cycles. Remarkably, the capacity can recover to the initial value at a low current density of 0.1 A g^{-1} after the high current density measurements, indicating the excellent reversibility and superior rate capability. In contrast, the CNT/meso-Si electrode exhibits a fast capacity fading after the second cycle, indicating that the meso-Si layer experiences a huge volume change and the capacity has an irreversible loss during the charge/discharge process (Figure S10). To further evaluate the cycling stability of the CNT/meso-Si/C electrode, the charge/discharge behavior of the cells for 500 cycles was recorded at the constant current density of 0.5 A g^{-1} (Figure 3e). It can be seen that the CNT/meso-Si/C composite electrode presents a high capacity of 2100 mAh g^{-1} for the first discharge. The capacity then stabilizes at about 1950 mAh g^{-1} after several cycles. A capacity of 1800 mAh g^{-1} is still remained after 500 cycles, demonstrating that the CNT/meso-Si/C composite electrode exhibits excellent cycling stability. The coulombic efficiencies of CNT/meso-Si/C electrode remain relatively low (~95%) in the first 50 cycles, which is attributed to the formation of instable SEI layer[26,28,31–33] at high current densities and also to the insufficient electrolyte immersion.[34,35] After that, the coulombic efficiency gradually increases to 99% and remains stable during the next cycles, indicating highly reversible conversion between the charge and discharge processes. For the practical applications, the low initial coulombic efficiencies should be improved. This excellent cycling stability is due to the carbon coating layer on the meso-Si that can accommodate large volume change in the charge/discharge process. It has been reported that the magnesium reduction process can reduce the Si volume to around 25–30% of the original SiO_2 components.[23] Thus, the volume of void space (generated during synthesis) inside the carbon layers is about three times that of meso-Si, which is large enough for the volume expansion of meso-Si during the Li insertion/extraction processes. The carbon coating layer

also can prevent the meso-Si from shedding and maintain the structural integrity. Therefore, the cycling stability of the CNT/meso-Si/C electrode has been significantly enhanced. To confirm this effect, the SEM and TEM images after 100 cycles were investigated (Figure 4a, 4b and 4c). As shown in Figure 4a, the porous characteristics and core-shell structure are well maintained. The TEM image shows that there were no obvious cracks in the meso-Si layer. The high resolution TEM image in Figure 4c indicates that the Si nanocrystals are still embedded inside the carbon layer, confirming that the flexible carbon layer can well confine and stabilize the meso-Si. This observation indicates that the porous structure and carbon coating layer can well reduce the stress derived from volume change during the lithiation and delithiation process.[23] These results demonstrate that the hierarchical structured CNT/meso-Si/C electrodes have potential as ideal candidate of LIB electrodes.

CONCLUSIONS

In summary, we designed a 3D hierarchical porous structured CNT/meso-Si/C composite by coating a uniform carbon-wrapped meso-Si throughout the CNT sponge by a magnesiothermic reduction approach. In this well-organized system, the hierarchical porous network with large pore volume and high surface area facilitates the Li^+ diffusion and electrolyte/electrode contact, and the flexible C coating layer alleviates the volume change of meso-Si during the charge/discharge process and simultaneously protects the structure integrity. Furthermore, the conductive CNT network serves as the current collector for efficient electrons and ions transportation. The excellent mechanical flexibility of CNT/meso-Si/C electrode also ensures the electrode integrity during the repeated charge/discharge process. When employed as LIBs electrode, the sandwiched CNT/meso-Si/C structure shows a high specific capacity of 2100 mAh g^{-1} at a current density of 0.1 A g^{-1}, superior

rate capability (81% of the initial capacity value) and cyclic stability (capacity remains as high as 1800 mAh g^{-1} after 500 cycles at a high current density of 0.5 A g^{-1}). The combination of 3D hierarchical porous CNT conductive network with high capacity meso-Si represents an effective strategy for developing efficient electrodes in various energy storage systems.

ASSOCIATED CONTENT

Supporting Information

SEM and TEM images of CNT, CNT/meso-SiO_2 and CNT/meso-Si/C sponges; TGA curves of CNT and CNT/meso-Si/C sponges; N_2 adsorption-desorption curves and pore size distributions of CNT/meso-Si/C sponges; Mechanical performance tests of CNT/meso-Si/C sponges; Charge-discharge curves and cycling performance of CNT sponges; Charge-discharge curves of CNT/meso-Si/C sponges with different meso-Si thicknesses; SEM image of the CNT/meso-Si/C sponge electrode after charge and discharge cycles; The Supporting Information is available free of charge *via* the Internet at http://pubs.acs.org.

AUTHOR INFORMATION

Corresponding Author

*anyuan@pku.edu.cn

*yuanquan@whu.edu.cn

NOTES

The authors declare no competing financial interest.

ACKNOWLEDGMENTS

This work was supported by the National Natural Science Foundation of China (51272186, 21422105, 21675120, 51325202), Wuhan Municipal Science and Technology Project (2014013001011283) and Ten Thousand Talents Program for Young Talents.

REFERENCES

1 Magasinski, A.; Dixon, P.; Hertzberg, B.; Kvit, A.; Ayala, J.; Yushin, G. High-Performance Lithium-Ion Anodes Using a Hierarchical Bottom-up Approach. *Nat. Mater.* **2010**, *9*, 353–358.

2 Jung, D. S.; Ryou, M. -H.; Sung, Y. J.; Park, S. B.; Choi, J. W. Recycling Rice Husks for High-Capacity Lithium Battery Anodes. *Proc. Natl. Acad. Sci. U. S. A.* **2013**, *110*, 12229–12234.

3 Si, W. P.; Yan, I. Mönch, C. L.; Deng, J. W.; Li, S. L.; Lin, G. G.; Han, L. Y.; Mei, Y. F.; Schmidt, O. G. A Single Rolled-Up Si Tube Battery for the Study of Electrochemical Kinetics, Electrical Conductivity, and Structural Integrity. *Adv. Mater*. **2014**, *26*, 7973–7978.

4 Yao, Y.; McDowell, M. T.; Ryu, I.; Wu, H.; Liu. N.; Hu, L.; Nix, W. D.; Cui, Y. Interconnected Silicon Hollow Nanospheres for Lithium-Ion Battery Anodes with Long Cycle Life. *Nano Lett.* **2011**, *11,* 2949–2954.

5 McDowell, M. T.; Lee, S. W.; Nix, W. D.; Cui, Y. 25th Anniversary Article: Understanding the Lithiation of Silicon and Other Alloying Anodes for Lithium-Ion Batteries. *Adv. Mater.* **2013**, *25,* 4966–4985.

6 Wang, C.; Wu, H.; Chen, Z.; McDowell, M. T.; Cui, Y.; Bao, Z. Self-Healing Chemistry Enables the Stable Operation of Silicon Microparticle Anodes for High-Energy Lithium-Ion Batteries. *Nat. Chem.* **2013**, *5,* 1042–1048.

7 Yi, R.; Dai, F.; Gordin, M. L.; Sohn, H.; Wang, D. H. Influence of Silicon Nanoscale Building Blocks Size and Carbon Coating on the Performance of Micro-Sized Si–C Composite Li-Ion Anodes. *Adv. Energy Mater.* **2013**, *3,* 1507–1515.

8 Zhang, Y. C.; You, Y.; Xin, S.; Yin, Y.-X.; Zhang, J.; Wang, P.; Zheng, X. S.; Cao, F. F.; Guo, Y. G. Rice Husk-Derived Hierarchical Silicon/Nitrogen-Doped Carbon/Carbon Nanotube Spheres as Low-Cost and High-Capacity Anodes for Lithium-Ion Batteries. *Nano Energy* **2016,** *25*, 120–127.

9 Jing, S. L.; Jiang, H.; Hu, Y. J.; Shen, J. H.; Li, C. Z. Face-to-Face Contact and Open-Void Coinvolved Si/C Nanohybrids Lithium-Ion Battery Anodes with Extremely Long Cycle Life. *Adv. Funct. Mater.* **2015,** *25*, 5395–5401.

10 Feng, X. J.; Yang, J.; Bie, Y. T.; Wang, J. L.; Nuli, Y.; Lu, W. Nano/Micro-Structured Si/CNT/C Composite from Nano-SiO_2 for High Power Lithium Ion Batteries. *Nanoscale* **2014,** *6*, 12532–12539.

11 Wang, B.; Li, X. L.; Zhang, X. F.; Luo, B.; Zhang, Y. B.; Zhi, L. J. Contact-Engineered and Void-Involved Silicon/Carbon Nanohybrids as Lithium-Ion-Battery Anodes. *Adv. Mater.* **2013,** *25*, 3560–3565.

12 Lin, H. J.; Weng, W.; Ren, J.; Qiu, L. B.; Zhang, Z. T.; Chen, P. N.; Chen, X. L.; Deng, J.; Wang, Y. G.; Peng, H. S. Twisted Aligned Carbon Nanotube/Silicon Composite Fiber Anode for Flexible Wire-Shaped Lithium-Ion Battery. *Adv. Mater.* **2014**, *26,* 1217–1222.

13 Ji, J.; Ji, H.; Zhang. L. L.; Zhao, X.; Bai, X.; Fan, X.; Zhang, F.; Ruoff, R. S. Graphene-Encapsulated Si on Ultrathin-Graphite Foam as Anode for High Capacity Lithium-Ion Batteries. *Adv. Mater.* **2013**, *25,* 4673–4677.

14 Fan, Y.; Zhang, Q.; Xiao, Q. Z.; Wang, X. H.; Huang, K. High Performance Lithium Ion Battery Anodes Based on Carbon Nanotube-Silicon Core-Shell Nanowires with Controlled Morphology. *Carbon* **2013,** *59*, 264–269.

15 Wang, W.; Epur, R.; Kumta, P. N. Vertically Aligned Silicon/Carbon Nanotube (VASCNT) Arrays: Hierarchical Anodes for Lithium-Ion Battery. *Electrochem. Commun.* **2011,** *13*, 429–432.

16 Cui, L. F.; Hu, L. B.; Choi, J. W.; Cui, Y. Light-Weight Free-Standing Carbon Nanotube-Silicon Films for Anodes of Lithium Ion Batteries. *ACS Nano* **2010,** *4*, 3671–3678.

17 Wang, W.; Ruiz, I.; Ahmed, K.; Bay, H. H.; George, A. S.; Wang, J.; Butler, J.; Ozkan, M.; Ozkan, C. S. Silicon Decorated Cone Shaped Carbon Nanotube Clusters for Lithium Ion Battery Anodes. *Small* **2014,** *10*, 3389–3396.

18 Wang, W.; Kumta, P. N. Nanostructured Hybrid Silicon/Carbon Nanotube Heterostructures: Reversible High-Capacity Lithium-Ion Anodes. *ACS Nano* **2010,** *4*, 2233–2241.

19 Fu, K.; Yildiz, O.; Bhanushali, H.; Wang, Y. X.; Stano, K.; Xue, L. G.; Zhang, X. W.; Bradford, P. D. Aligned Carbon Nanotube-Silicon Sheets: A Novel Nano-Architecture for Flexible Lithium Ion Battery Electrodes. *Adv. Mater.* **2013,** *25*, 5109–5114.

20 Xiao, L. S.; Sehlleier, Y. H.; Dobrowolny, S.; Orthner, H.; Mahlendorf, F.; Heinzel, A.; Schulz, C.; Wiggers, H. Si-CNT/RGO Nanoheterostructures as High-Performance Lithium-Ion-Battery Anodes. *ChemElectroChem* **2015,** *2*, 1983–1990.

21 Wang, B.; Li, X. L.; Zhang, X. F.; Luo, B.; Jin, M. H.; Liang, M. H.; Dayeh, S. A.; Picraux, S. T.; Zhi, L. J. Adaptable Silicon-Carbon Nanocables Sandwiched between Reduced Graphene Oxide Sheets as Lithium Ion Battery Anodes. *ACS Nano* **2013,** *7*, 1437–1445.

22 Fan, Y.; Zhang, Q.; Lu, C. X.; Xiao, Q. Z.; Wang, X. H.; Tay, B. K. High Performance Carbon Nanotube-Si Core-Shell Wires with a Rationally Structured Core for Lithium Ion Battery Anodes. *Nanoscale* **2013,** *5*, 1503–1506.

23 Zhang, R. Y.; Du, Y. J.; Li, D.; Shen, D. K.; Yang, J. P.; Guo, Z. P.; Liu, H. K.; Elzatahry, A. A.; Zhao, D. Y. Highly Reversible and Large Lithium Storage in Mesoporous Si/C Nanocomposite Anodes with Silicon Nanoparticles Embedded in a Carbon Framework. *Adv. Mater.* **2014**, *26,* 6749–6755.

24 Gui, X. C.; Wei, J. Q.; Wang, K. L.; Cao, A. Y.; Zhu, H. W.; Jia, Y.; Shu, Q. K.; Wu, D. H. Carbon Nanotube Sponges. *Adv. Mater.* **2010**, *22,* 617–621.

25 Yang, Y. B.; Shi, E. Z.; Li, P. X.; Wu, D. H.; Wu, S. T.; Shang, Y. Y.; Xu, W. J.; Cao, A. Y.; Yuan, Q. A Compressible Mesoporous SiO_2 Sponge Supported by a Carbon Nanotube Network. *Nanoscale* **2014**, *6,* 3585–3592.

26 Kim, W.-S.; Choi, J.; Hong, S.-H. Meso-Porous Silicon-Coated Carbon Nanotube as an Anode for Lithium-Ion Battery. *Nano Res.* **2016**, *9,* 2174–2181.

27 Evanoff, K.; Benson, J.; Schauer, M.; Kovalenko, I.; Lashmore, D.; Ready, W. J.; YuShin, G. Ultra Strong Silicon-Coated Carbon Nanotube Nonwoven Fabric as a Multifunctional Lithium-Ion Battery Anode. *ACS Nano* **2012**, *6,* 9837–9845.

28 Du, F.-H.; Li, B.; Fu, W.; Xiong, Y.-J.; Wang, K.-X.; Chen, J. -S. Surface Binding of Polypyrrole on Porous Silicon Hollow Nanospheres for Li-Ion Battery Anodes with High Structure Stability. *Adv. Mater.* **2014**, *26,* 6145–6150.

29 Bang, B. M.; Lee, J. I.; Kim, H.; Cho, J.; Park, S. High-Performance Macroporous Bulk Silicon Anodes Synthesized by Template-Free Chemical Etching. *Adv. Energy Mater.* **2012**, *2,* 878–883.

30 Kim, H.; Han, B.; Choo, J.; Cho, J. Three-Dimensional Porous Silicon Particles for Use in High-Performance Lithium Secondary Batteries. *Angew. Chem. Int. Ed.* **2008**, *47,* 10151–10154.

31 Zhao, J.; Lee, H.-W.; Sun, J.; Yan, K.; Liu, Y. Y.; Liu, W.; Lu, Z. D.; Lin, D. C.; Zhou, G. M.; Cui, Y. Metallurgically Lithiated SiO_x Anode with High Capacity and Ambient Air Compatibility. *Proc. Natl. Acad. Sci. U. S. A.* **2016,** *113*, 7408–7413.

32 Rehnlund, D.; Lindgren, F.; Böhme, S.; Nordh, T.; Zou, Y. M.; Pettersson, J.; Bexell, U.; Boman, M.; Edström, K.; Nyholm, L. Lithium Trapping in Alloy Forming Electrodes and Current Collectors for Lithium Based Batteries. *Energy Environ. Sci.* **2017,** DOI: 10.1039/c7ee00244k.

33 Ko, M.; Chae, S.; Ma, J.; Kim, N.; Lee, H.-W.; Cui, Y.; Cho, J. Scalable Synthesis of Silicon-Nanolayer-Embedded Graphite for High-Energy Lithium-Ion Batteries. *Nat. Energy* **2016,** *1*, 16113.

34 Hu, L. B.; Wu, H.; Gao, Y. F.; Cao, A. Y.; Li, H. B.; McDough, J.; Xie, X.; Zhou, M.; Cui, Y. Silicon-Carbon Nanotube Coaxial Sponge as Li-Ion Anodes with High Areal Capacity. *Adv. Energy Mater.* **2011,** *1*, 523–527.

35 Evanoff, K.; Khan, J.; Balandin, A. A.; Magasinski, A.; Ready, W. J.; Fuller, T. F.; Yushin, G. Towards Ultrathick Battery Electrodes: Aligned Carbon Nanotube-Enabled Architecture. *Adv. Mater.* **2012,** *24*, 533–537.

36 Zhang, Z. L.; Wang, Y. H.; Ren, W. F.; Tan, Q. Q.; Chen, Y. F.; Li, H.; Zhong, Z. Y.; Su, F. B. Scalable Synthesis of Interconnected Porous Silicon/Carbon Composites by the Rochow Reaction as High-Performance Anodes of Lithium Ion Batteries. *Angew. Chem. Int. Ed.* **2014**, *126,* 5265–5269.

37 Park, Y.; Choi, N. S.; Park, S.; Woo, S. H.; Sim, S.; Jang, B. Y.; Oh, S. M.; Park, S.; Cho, J.; Lee, K. T. Si-Encapsulating Hollow Carbon Electrodes *via* Electroless Etching for Lithium-Ion Batteries. *Adv. Energy Mater.* **2013**, *3,* 206–212.

38 Jia, H.; Gao, P.; Yang, J.; Wang, J.; Nuli, Y.; Yang, Z. Novel Three-Dimensional Mesoporous Silicon for High Power Lithium-Ion Battery Anode Material. *Adv. Energy Mater.* **2011**, *1,* 1036–1039.

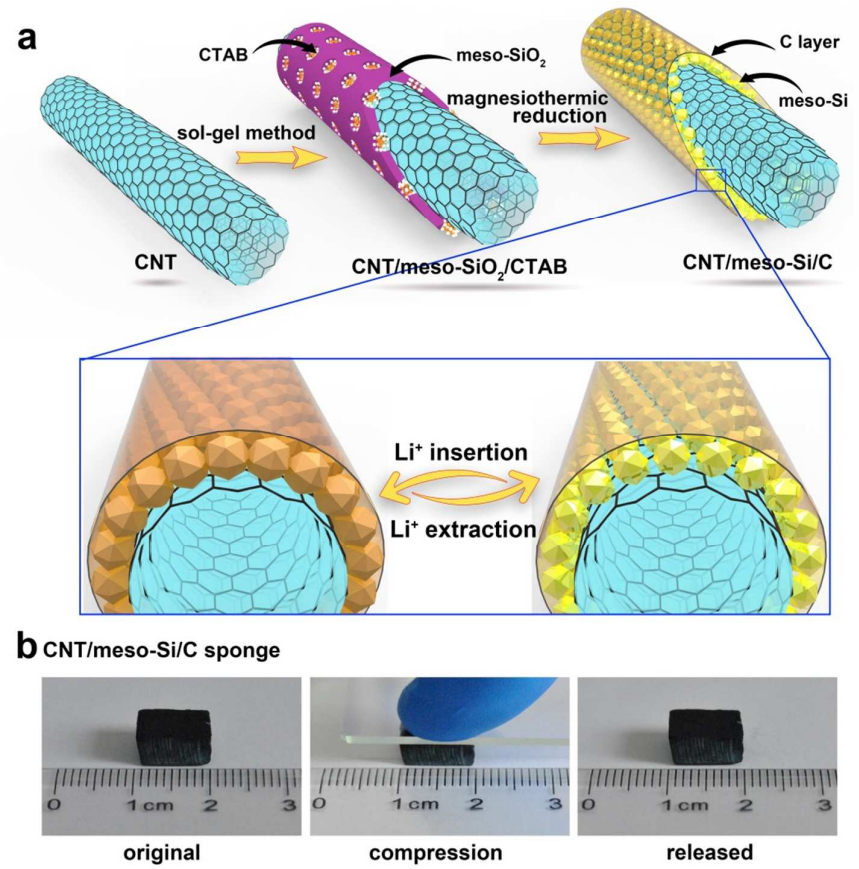

Figure 1. (a) Schematic illustration of the fabrication process of CNT/meso-Si/C nanocomposite by magnesiothermic reduction approach. (b) Photos of CNT/meso-Si/C sponges under different deformations.

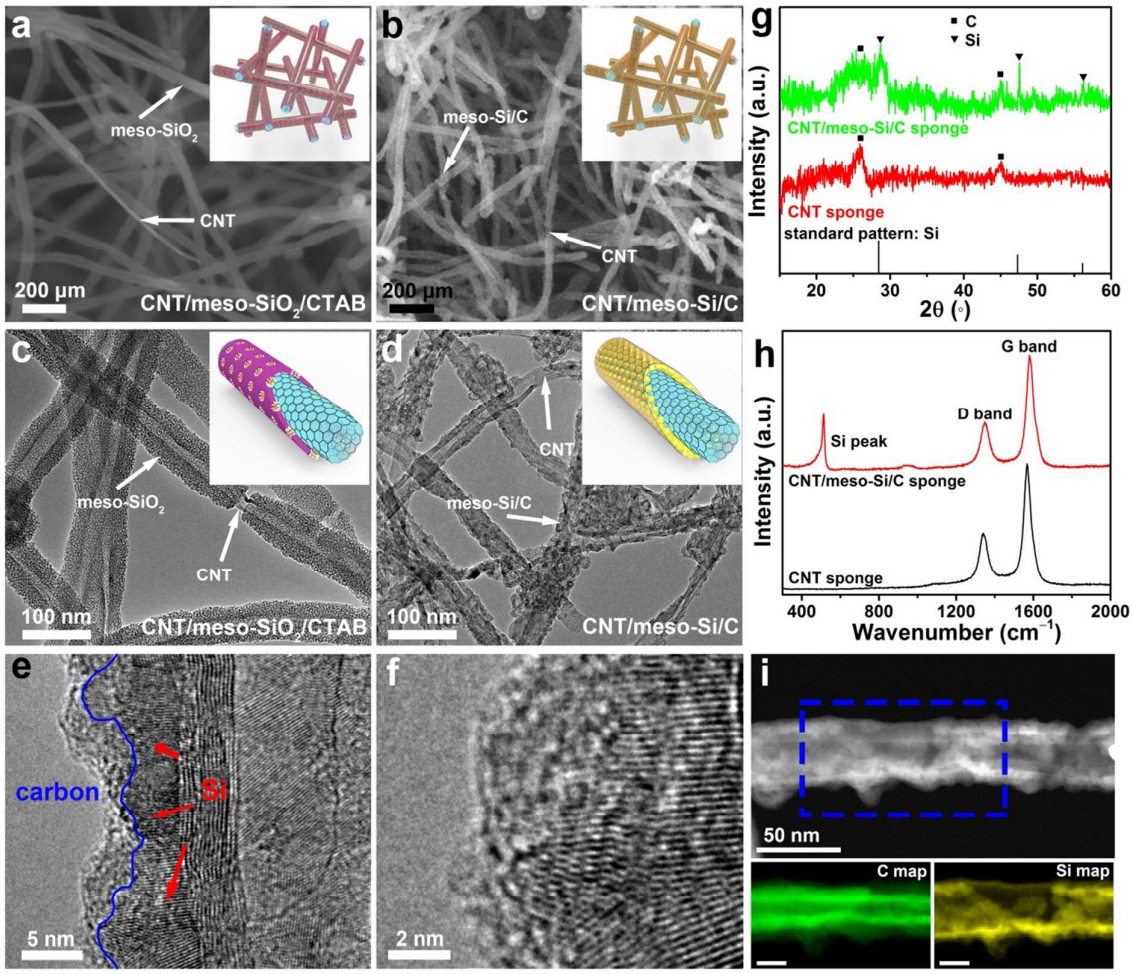

Figure 2. Structural characterization of composite sponges. SEM images of (a) CNT/meso-SiO_2/CTAB and (b) CNT/meos-Si/C composite sponges. Insets of (a, b) are structural models of porous CNT/meso-SiO_2/CTAB and CNT/meso-Si/C sponges. TEM images of (c) CNT/meso-SiO_2/CTAB and (d) CNT/meos-Si/C core-shell structure. Insets of (c, d) are structural models of CNT/meso-SiO_2/CTAB and CNT/meso-Si/C core-shell structure. (e) High resolution TEM image of CNT/meso-Si/C nanocomposite. (f) The magnified image of meso-Si. (g) XRD patterns of the CNT, CNT/meso-Si/C and the standard pattern of Si. (h) Raman spectra of the CNT and CNT/meso-Si/C sponges. (i) Dark-field image and the corresponding C and Si elemental mapping of the CNT/meso-Si/C sandwiched structure. Scale bars in the elemental mapping images are 20 nm.

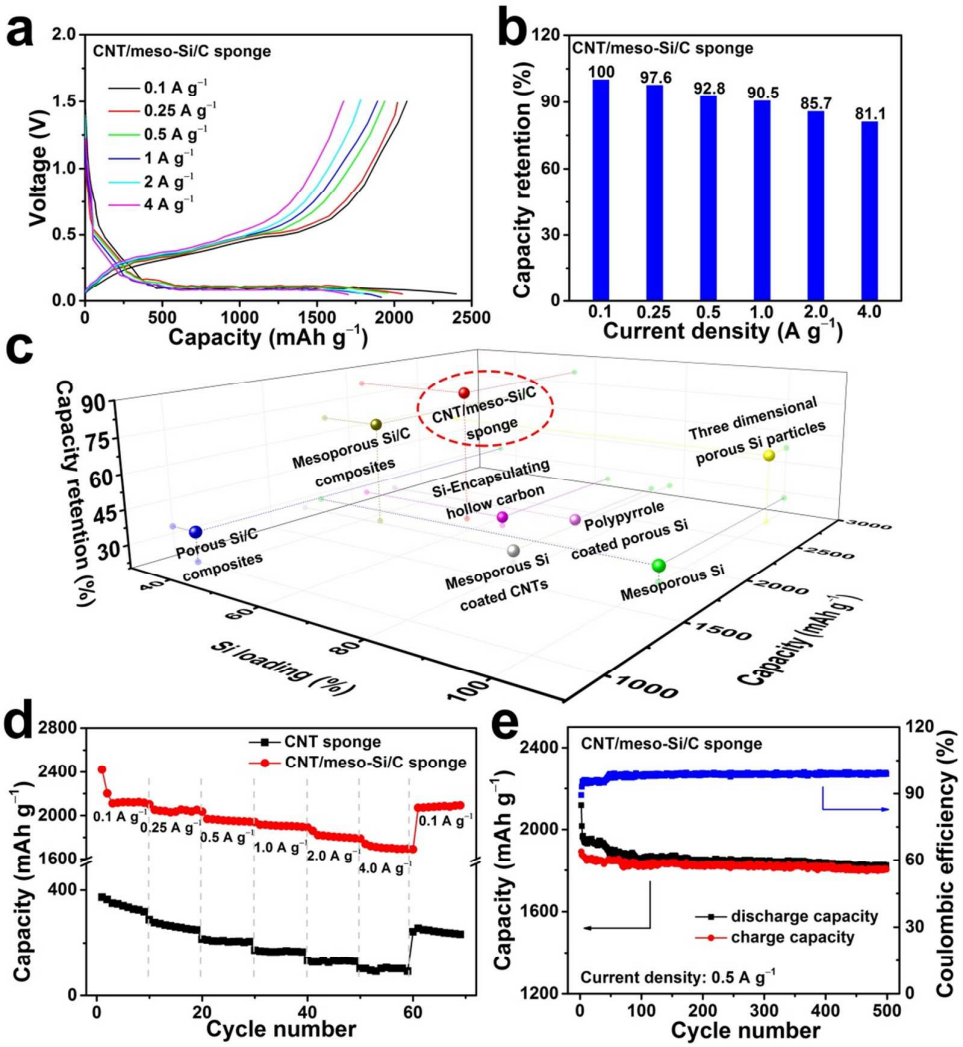

Figure 3. (a) Galvanostatic charge/discharge profiles of the CNT/meso-Si/C electrode at a variety of current densities from 0.1 to 4 A g^{-1}. The calculation is based on the whole electrode material including CNT and meso-Si. (b) Capacity retention of the CNT/meso-Si/C electrode at various current densities. (c) Comparison of the LIBs performance between CNT/meso-Si/C sponge electrode and several reported Si-based electrodes such as porous Si/C composites,[36] mesoporous Si/C composites,[23] Si-encapsulating hollow carbon,[37] mesoporous Si coated CNTs,[26] polypyrrole coated porous Si,[28] mesoporous Si,[38] and three dimensional porous Si particles.[30] Data taken from refs 36, 23, 37, 26, 28, 38, 30. (d) The cycling and rate capabilities of CNT/meso-Si/C electrode at various current densities from 0.1 to 4 A g^{-1}. (e) The charge, discharge capacity and coulombic efficiency of the CNT/meso-Si/C electrode *versus* cycle number at the current density of 0.5 A g^{-1}.

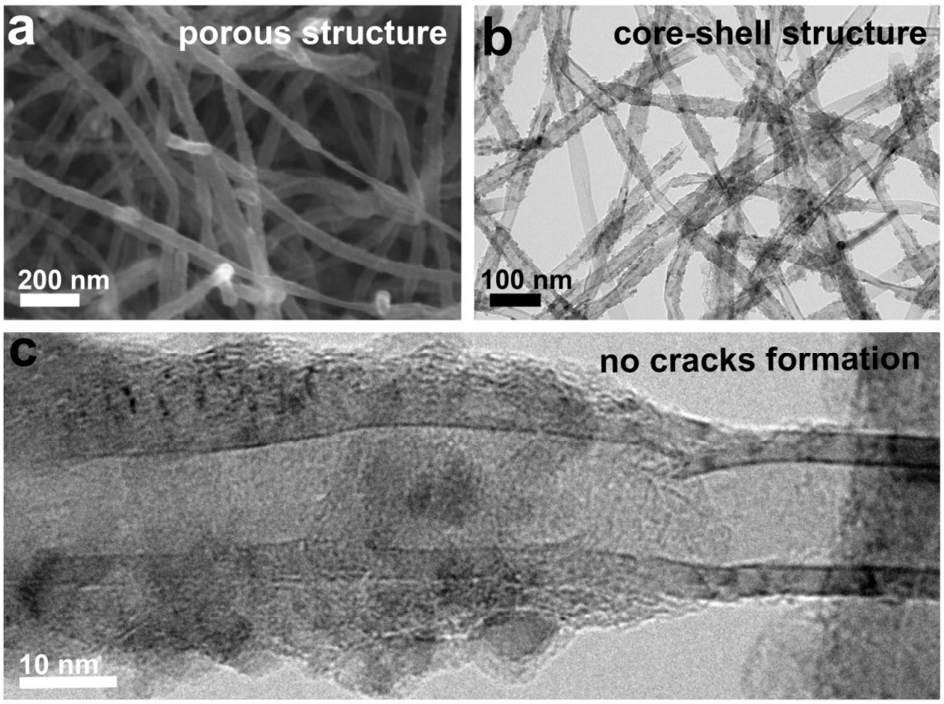

Figure 4. (a) SEM, (b) TEM and (c) High resolution TEM images of the CNT/meso-Si/C electrode after 100 charge/discharge process at a cycling rate of 1 A g^{-1}.

TABLE of CONTENTS